N-cadherin facilitates trigeminal sensory neuron outgrowth and target tissue innervation

Caroline A. Halmi[1], Alec T. McIntosh[2], Carrie E. Leonard[1], Lisa A. Taneyhill[1,*]

[1]Department of Animal and Avian Sciences, University of Maryland, College Park, MD 20742 USA

[2]Lombardi Comprehensive Cancer Center, Georgetown University, Washington, DC, 20007 USA

*corresponding author

Email: ltaney@umd.edu

Keywords: Trigeminal ganglion, neural crest, placode cells, N-cadherin, pioneer neurons.

Abstract

During embryonic development, diverse cell types coordinate to form functionally complex tissues. Exemplifying this process, the trigeminal ganglion emerges from the condensation of two distinct precursor cell populations, cranial placodes and neural crest, with neuronal differentiation of the former preceding the latter. While the dual origin of the trigeminal ganglion has been understood for decades, the molecules orchestrating formation of the trigeminal ganglion from these precursors remain relatively obscure. Initial assembly of the trigeminal ganglion is mediated by cell adhesion molecules, including neural cadherin (N-cadherin), which is required by placodal neurons to properly condense with other neurons and neural crest cells. Whether N-cadherin is required for later growth and target innervation by trigeminal ganglion neurons, however, is unknown. To this end, we depleted N-cadherin from chick trigeminal placode cells and uncovered decreases in trigeminal ganglion size, nerve growth, and target innervation *in vivo* at later developmental stages. Furthermore, blocking N-cadherin-mediated adhesion prevented axon extension in some placode-derived trigeminal neurons *in vitro*. This indicates the existence of neuronal subtypes that may have unique requirements for N-cadherin for outgrowth, and points to this subset of placodal neurons as potential pioneers that serve as templates for additional axon outgrowth. Neurite complexity was also decreased in neural crest-derived neurons *in vitro* in response to N-cadherin knockdown in placode cells. Collectively, these findings reveal persistent cell autonomous and non-cell autonomous functions for N-cadherin, thus highlighting the critical role of N-cadherin in mediating reciprocal interactions between neural crest and placode neuronal derivatives during trigeminal ganglion development.

Significance Statement

Our findings are significant because they demonstrate how neurons derived from two distinct cell populations, neural crest and placode cells, coordinate the outgrowth of their axons in time and space to generate the trigeminal ganglion using the cell adhesion molecule N-cadherin. Notably, our results provide evidence for the existence of subpopulations of neurons within the trigeminal ganglion that differentially require N-cadherin to facilitate axon outgrowth, and hint at the possibility that trigeminal pioneer neurons are derived from placode cells while followers arise from both placode and neural crest cells. These studies provide new insight into trigeminal gangliogenesis that will likely be translatable to other cranial ganglia and vertebrate species.

Introduction

The cranial ganglia and their associated nerves are critical for integrating various sensory inputs, transmitting this information to the brain to allow for an appropriate response. Sensory signals are detected by neurons whose cell bodies reside in the ganglia and whose axons project throughout the body where they facilitate diverse functions such as somatosensation and the innervation of visceral organs. The trigeminal nerve, the largest and most complex of the twelve paired cranial nerves, relays the majority of somatosensory information within the head. The trigeminal nerve is composed of three major branches - the ophthalmic (OpV), maxillary (MxV), and mandibular (MnV) - that innervate the forehead and eye region, upper jaw, and lower jaw, respectively. While all three branches relay sensory information, only the mandibular branch has motor neurons that aid in mastication.

The chick embryo is an exemplary model for understanding developmental processes, including discerning the cell types that comprise the trigeminal ganglion[1,2]. Both neural crest cells and neurogenic placode cells contribute neurons to the trigeminal ganglion[2], while the neural crest also gives rise to glial cells. Neural crest cells that contribute to the trigeminal ganglion originate from the midbrain and anterior hindbrain[3,4]; however, the neural crest as a cell population are found throughout the body axis and are capable of differentiating into an array of cell types including cranial bone and cartilage, melanocytes, and cardiac myocytes[5,6]. Neurogenic placodes are specialized regions of thickened ectoderm that differentiate into neurons. Initially, there is slight overlap between the different placodes that comprise the cranial ganglia; however, as development progresses, the placodes become more segregated and distinct[7]. The trigeminal placode consists of the OpV and maxillomandibular (MmV) placodes, which form all placode-derived neurons of the trigeminal ganglion. Although OpV and MmV placodes eventually produce one structure, they differ from one another in two important ways. First, OpV and MmV placodes contribute neurons to distinct lobes of the trigeminal ganglion (OpV, and MxV and MnV, respectively). Second, most of the neurons to which the OpV placode gives rise are post-mitotic prior to delamination, traveling to the trigeminal ganglion-forming region as differentiated neurons. Conversely, the MmV placode generates neuroblasts that do not differentiate or become post-mitotic until they reach ganglionic anlage[8–11]. Notably, in the chick, placodal neurons are the first neurons present within the trigeminal ganglion, differentiating and growing towards the periphery to make initial connections with their targets within 2-5 days of development. In contrast, neural crest cells only begin neuronal differentiation at 4 days of development, and continue differentiating up to 7 days[1,12].

Reciprocal interactions between neural crest cells and placodal neurons are required to properly form the trigeminal ganglion[2,13,14]. The bulk of this research has focused on the influence of neural crest cells on surrounding cell types, placode cells included, but there is limited knowledge about how placodal neurons influence the neural crest. Because placodal neurons differentiate

prior to neural crest-derived neurons, there is the intriguing possibility that they serve as pioneer neurons, the earliest populations of neurons within a system that innervate targets and provide a scaffold for later-born neurons to grow along[15]. While much of the evidence for pioneer neurons comes from invertebrate models[16–19], some evidence exists in vertebrates[20–22], including studies of trigeminal neurodevelopment[23]. Within the chick, the use of a monoclonal antibody against tubulin beta 3, class III (Tubb3) uncovered that placode cells express Tubb3 before they leave the ectoderm, while neural crest cells express Tubb3 later upon becoming neurons[24], in keeping with findings on the timeline of trigeminal sensory neuron differentiation. This cumulative knowledge suggests that placodal neurons may be pioneers that serve as templates upon which later differentiating neural crest-derived neurons extend axons[24]; however, additional evidence for this is needed, and molecules orchestrating this process remain unknown.

Intercellular adhesion among placode cells and neural crest cells in part regulates gangliogenesis[25], and could therefore also function in facilitating trigeminal axon outgrowth to targets. Specifically, cadherins promote adhesion between adjacent cells and are known mediators of gangliogenesis[26–28]. The cadherin extracellular domain facilitates *cis* and *trans* interactions via homophilic and heterophilic binding[26,29,30] while the intracellular domain contains two binding sites for catenin proteins (p120-catenin and β-catenin) that regulate its adhesive ability and provide a link to the actin cytoskeleton, respectively[31]. Neural cadherin (N-cadherin) is expressed in neural tissue at various stages of development[32], and in mesodermal[33,34] and ectodermal derivatives, including trigeminal and epibranchial placode cells prior to their delamination[35]. During neurodevelopment, N-cadherin possesses important roles in regulating neurite formation[36], axon fasciculation, and synapse formation[37–40]. While N-cadherin function in placode cells is critical for the initial condensation of the trigeminal ganglion[35], whether N-cadherin mediates the later growth and maturation of trigeminal ganglion neurons, and specifically neurite production and axon extension, is unknown. Furthermore, how N-cadherin-expressing placodal neurons impact the development of neural crest-derived neurons is poorly understood.

Here, we demonstrate that placodal expression of N-cadherin is important throughout gangliogenesis, with defects to morphology observed in both the ganglion and axonal projections to target tissues upon N-cadherin depletion from placode cells. Additionally, we show a reduction in axonal projections *in vivo* and *in vitro* that can be attributed to a loss of N-cadherin-mediated adhesion. Strikingly, we note decreased neurite production in neural crest-derived neurons, indicating non-cell autonomous effects on the neural crest after N-cadherin knockdown in placodal neurons. These results suggest that the majority of trigeminal neurons depend on the adhesive function of N-cadherin, initially expressed in placodal neurons, to facilitate the outgrowth of their axons, and uncover the existence of a subpopulation of placodal neurons that do not rely on N-cadherin-mediated adhesion, which could be the true pioneer neurons of the trigeminal ganglion.

Altogether, our findings reveal a new long-term role for N-cadherin, which is initially only expressed and utilized by placodal neurons, in driving the proper outgrowth of both placode- and neural crest-derived neurons throughout trigeminal gangliogenesis.

Results

N-cadherin knockdown in placode cells disrupts trigeminal ganglion development

While the expression of N-cadherin in cranial placode cells as well as sensory and motor neurons has been established[41–44], along with N-cadherin function in early trigeminal ganglion assembly[27], the role of N-cadherin in later trigeminal ganglion development in both placode- and neural crest-derived neurons is unknown. To elucidate the function of N-cadherin-expressing placodal neurons in the formation and maturation of the trigeminal ganglion, a validated N-cadherin morpholino (MO) was unilaterally electroporated into trigeminal placode cells prior to their delamination[27]. Initial experiments with a 5 base pair mismatch N-cadherin control MO (N-cadherin MM)[27] were performed to compare electroporated and contralateral trigeminal ganglia (Supplemental Figure 1) to ensure the electroporation technique did not cause any morphological changes. Once this was confirmed, the unelectroporated (contralateral) sides of N-cadherin MO-electroporated embryos were used as controls to account for size variation among embryos that arises during development.

Trigeminal ganglion size and nerve morphology in electroporated embryos were analyzed at various developmental stages by whole-mount immunohistochemistry using an antibody against Tubb3 to label neurons, followed by tissue clearing to render samples transparent for imaging. Because neural crest cells begin differentiating into neurons starting at embryonic day 4 (E4/ HH23)[12,24], it was assumed that the Tubb3 antibody identified only placode-derived neurons up to E4 while afterwards labeled neuronal contributions from both cell types indistinguishably.

During initial gangliogenesis (E2.5/HH16-18), N-cadherin depletion from trigeminal placode cells led to more dispersed neurons and increased the area of the forming trigeminal ganglion compared to the unelectroporated contralateral side (Figure 1A-A', 1E). These results recapitulated previous work that showed knockdown of N-cadherin in trigeminal placode cells impacted proper aggregation of trigeminal placodal neurons with each other and with undifferentiated neural crest cells in early gangliogenesis [27]. In contrast, following the condensation of the trigeminal ganglion 24 hours later in development (E3.5/HH19-22), the opposite phenotype was observed. We noted a statistically significant reduction in the size of the trigeminal ganglion on the electroporated side compared to the contralateral control (Figure 1B-B', 1E). As neural crest cells start differentiating into neurons (E4.5/HH23-25), this reduced size persisted (Figure 1C-C', 1E). Finally, at both E5.5 (HH26-27) and E6.5 (HH28-30), N-cadherin MO-electroporated trigeminal

ganglia were no longer statistically different from unelectroporated contralateral trigeminal ganglia (Figure 1D-D', 1E).

Following the results from the whole trigeminal ganglion surface area measurements, we next sought to discern whether N-cadherin had differential importance within the OpV and the MmV placodes, as these placodes arise distinctly from one another[9,10]. Interestingly, N-cadherin knockdown led to a statistically significant increase in dispersal of MmV neurons at E2.5 (HH16-18), with no impact to OpV neurons (Figure 1F-G). However, throughout the remaining stages examined (E3.5-E5.5, HH19-HH27), N-cadherin depletion did not affect MmV lobe development (Figure 1G). Conversely, there was a statistically significant reduction in OpV lobe size (Figure 1F), correlating with visual observations (Figure 1D-D'). At E6.5 (HH28-30), the size of both lobes was not statistically different from unelectroporated contralateral lobes (Figure 1F-G). Given the drastic effects of N-cadherin knockdown on OpV compared to MmV (Figure 1F-G), we chose to focus our subsequent analyses on the development of the OpV lobe.

To assess whether the decreased size of the trigeminal ganglion was due to aberrant cell death and/or a change in the number of neural crest cells, apoptotic cells were quantified via TUNEL assay and immunohistochemistry was performed for the neural crest nuclear marker, Sox10, respectively. Only the stage groupings that showed significant differences in size were examined (E2.5/HH16-18, E3.5/HH19-22, E4.5/HH23-25). These experiments revealed no differences in cell death or neural crest cell number between the contralateral and N-cadherin MO-treated side (Supplemental Figure 2), indicating that these parameters were not driving the observed morphological changes.

Depletion of N-cadherin from trigeminal placode cells disrupts target innervation by OpV nerves

Since increased cell death and changes in neural crest cell number could not explain the reduction in OpV lobe size, we evaluated whether OpV nerve projections into cranial target tissues might be impacted instead. We first examined the lateral nasal branch at E4.5 (HH23-25), as by this point, the branch is a prominent structure within the embryonic head[45]. To this end, we performed whole-mount Tubb3 immunohistochemistry, which labels both placodal and neural crest-derived neurons at this stage. These experiments revealed substantially fewer lateral nasal nerve axons after N-cadherin MO treatment compared to the contralateral side (Figure 2A-B). To quantify these findings, we first assessed the distribution of lateral nasal nerve axons at 30 μm intervals across each image, starting at the first point in the image where axon branching occurred from the OpV lobe. More proximal to the trigeminal ganglion, there was no difference in the number of axons. In contrast, fewer axons were present in distal regions of N-cadherin MO-treated lateral

nasal nerves (Figure 2C). Moreover, nerve width and innervation area were also significantly reduced after N-cadherin knockdown compared to controls (Figure 2D-E).

Additionally, we used Tubb3 immunohistochemistry to evaluate the medial nasal nerve, which begins to form in E4.5 (HH23-25) stage embryos[45]. Due to the increased variability in the development of this branch during these stages, we examined the E5.5 (HH26-27) stage grouping instead as these embryos possessed more consistent morphological development. The number of medial nasal nerve endings was similar between conditions (Figure 2F-H), yet the nerve width and target innervation area were significantly smaller after N-cadherin knockdown (Figure 2I-J). Together, these results reveal that N-cadherin is required by some individual OpV trigeminal neurons to send axons to targets, thus leading to proper nerve outgrowth, fasciculation, and target innervation, Further, individual nerve branches may be differentially affected by depletion of N-cadherin from trigeminal placode cells since the medial nasal nerve was impacted to a lesser extent than the lateral nasal nerve.

N-cadherin is important for proper axon outgrowth of some trigeminal neurons *in vitro*

Given the observed phenotypes *in vivo,* we hypothesized that trigeminal axon outgrowth was facilitated by N-cadherin in an adhesion-dependent manner. If trigeminal neurons express less N-cadherin, they may not properly adhere to each other, leading to deficiencies in axon extension and target innervation. To test this, we utilized a validated function-blocking antibody against the extracellular domain of N-cadherin, known as MNCD2[44,46] (anti-N-cadherin), to block N-cadherin-mediated adhesion in explanted trigeminal ganglion tissue. Explants were cultured *in vitro* for 24 hours, then treated with anti-N-cadherin or a rat IgG control antibody for 24 hours, followed by Tubb3 immunostaining and analysis (Figure 3A). Qualitatively, more axons appeared to grow out in control explants (Figure 3B) compared to anti-N-cadherin-treated explants (Figure 3B'). Ridge detection processing of images was then conducted to detect segments which were used as a proxy for individual axons (Figure 3C-C'), and then an intersection analysis was run to measure changes to axon outgrowth (Figure 3D-D'). We observed a reduction in the amount of Tubb3 fluorescence in the anti-N-cadherin-treated samples (Figure 3E), indicating decreased axon density in trigeminal ganglion explants after blocking N-cadherin-based adhesion. Furthermore, our intersection analysis revealed a diminished number of axonal projections in the anti-N-cadherin-treated explants (Figure 3F). Interestingly, of the neurons that did grow, the average length of a single axon was similar between conditions (Figure 3G), signifying that some trigeminal neurons can properly grow out to the periphery independent of N-cadherin function. Collectively, these findings suggest N-cadherin-mediated adhesion promotes axonal outgrowth and complexity in trigeminal neurons *in vitro*, and that dependence on N-cadherin function may differ in distinct neuronal subtypes.

A subset of placodal trigeminal neurons do not rely on N-cadherin for outgrowth

Since placodal neurons are the first neuronal population present in the trigeminal ganglion, we hypothesized that the neurons in our explant cultures that did not rely on N-cadherin-mediated adhesion for their outgrowth were of placodal origin. To test this, an ectodermal co-electroporation was performed using a genome-incorporating vector (PiggyBac) and its accompanying transposase (PBase)[47,48] that results in the stable expression of red fluorescent protein (PiggyBacRFP) in order to label placode-derived neurons. RFP-positive explants were cultured and treated with either rat IgG or anti-N-cadherin as previously described. Following immunostaining with Tubb3 and RFP antibodies, low magnification images revealed robust axon outgrowth, the majority of which overlapped with RFP-positive placode-derived neurons after rat IgG treatment (Figure 4A), whereas explants treated with anti-N-cadherin had reduced overall axon outgrowth and fewer RFP-positive projections (Figure 4C). Many Tubb3-positive projections were also RFP-positive in rat IgG-treated explants (Figure 4B-B”). This colocalization was maintained in the anti-N-cadherin-treated axonal projections; however, the total amount of outgrowth was less (Figure 4D-D”). While there was an overall reduction in the amount of Tubb3 fluorescence in the anti-N-cadherin-treated explants, indicating fewer axons after blocking N-cadherin-mediated adhesion, there was no change in the amount of RFP signal between the two treatment groups (Figure 4E). These findings reveal that blocking N-cadherin-mediated adhesion did not negatively affect the placodal neuron population as a whole, with N-cadherin instead functioning to facilitate axon outgrowth.

Given these findings and our prior results pointing to a role for N-cadherin in axon outgrowth, we hypothesized that anti-N-cadherin-treated explants would have a greater amount of RFP signal within the explanted tissue due to the presence of placodal neurons unable to extend axons in the absence of N-cadherin-mediated adhesion. To address this, we evaluated the RFP signal found in neuronal projections versus RFP signal remaining within the explant (Figure 4F). While 33% of the total RFP signal came from axonal projections in rat IgG-treated explants, this dropped to 13% in anti-N-cadherin-treated explants. In contrast, 67% of the total RFP signal was found in the explanted tissue in rat IgG-treated explants while 87% of the total RFP signal was observed in the explanted tissue in anti-N-cadherin-treated explants. Taken together, these data reveal that while more placodal neurons can extend axons when N-cadherin-mediated adhesion is functional, there is still a subset of placodal neurons that grow irrespective of N-cadherin.

Non-cell autonomous effects on neurite number and complexity in neural crest-derived neurons are observed after N-cadherin knockdown in placode cells

The overt changes in trigeminal axon outgrowth after reducing N-cadherin function both *in vivo* and *in vitro* led us to speculate that N-cadherin expression in placodal neurons was impacting

the other neuronal population of the trigeminal ganglion, later-born neural crest-derived neurons. To test this hypothesis, a sequential electroporation was performed to first label neural crest cells with a stably expressed green fluorescent protein (PiggyBacGFP plus PBase), followed by electroporation of placode cells with N-cadherin MO or N-cadherin MM. Sequentially-labeled explants were cultured *in vitro* for 3 days and were subsequently processed for immunostaining with GFP and Tubb3 antibodies (Figure 5A). Remarkably, we observed relatively few GFP-positive neural crest-derived axons in N-cadherin MO-treated samples, whereas N-cadherin MM-treated explants exhibited a higher prevalence of axons from neural crest-derived neurons (Supplemental Figure 3). Moreover, the axons in N-cadherin MM-treated explants emerged from the explants and created branch networks with other axons. These observations were not found in N-cadherin MO-treated explants. Interestingly, neurites, which precede axon specification and extension[49], were noted in GFP-positive neural crest-derived somata in both N-cadherin MO- and N-cadherin MM-treated explants. While N-cadherin MM-treated explants had numerous neurites per GFP-positive neural crest soma (Figure 5B', 5C), those in explants treated with N-cadherin MO had noticeably fewer (Figure 5D', 5E). Not only was there a significant decrease in the number of primary and secondary neurites in neural crest-derived neurons in N-cadherin MO-treated explants, tertiary neurites were absent even though they were observed in N-cadherin MM-treated explants (Figure 5F). Although neurite branching was deficient in N-cadherin MO-treated explants, there was no difference in the length of primary and secondary neurites compared to N-cadherin MM-treated explants (Figure 5G). These results indicate that N-cadherin in placodal neurons facilitates extension and branching of axons in neural crest-derived neurons *in vitro.* Altogether, our findings reveal that N-cadherin has cell autonomous and non-cell autonomous roles in placode- and neural crest-derived trigeminal neurons, respectively, thus facilitating proper morphology, outgrowth, and target innervation of the trigeminal nerve.

Discussion

During neurodevelopment, cells experience several environmental changes as they differentiate into specialized neurons. The first neurons that extend axons to target tissues, termed pioneers, set the path that later-born neurons will use as a template. Here we demonstrate a sustained role for N-cadherin during trigeminal gangliogenesis that highlights the importance of cell-cell adhesion during the formation and subsequent maturation of the OpV lobe of the trigeminal nerve. Our findings show that reducing N-cadherin from trigeminal placode cells and their neuronal derivatives leads to altered trigeminal ganglion morphology and deficient target innervation by specific OpV nerve branches. Intriguingly, these phenotypes cannot be attributed to aberrant apoptosis nor changes in the number of neural crest cells present within the trigeminal ganglion. We found that N-cadherin-mediated adhesion is necessary for the outgrowth of the majority but not

all placode- and neural crest-derived trigeminal neurons, with a subpopulation of the former functioning independently of N-cadherin, and perhaps serving as the pioneer neurons of the trigeminal ganglion.

Depletion of N-cadherin from placodal neurons leads to morphological defects in the developing trigeminal ganglion

Although a role for N-cadherin-expressing placode cells has been shown during the initial coalescence of neural crest and placodal neurons to generate the trigeminal ganglion[27], whether N-cadherin further regulates the ability of trigeminal neurons to extend axons to properly innervate their targets is not understood. Through our experiments, we showed that N-cadherin knockdown first increased ganglion surface area during early gangliogenesis, replicating previously published results[27], but then led to a reduction in trigeminal ganglion size up to 4.5 days into development, which eventually recovered. We believe there are two likely reasons for this recovery. First, MOs are typically only stable for up to 4-5 days *in vivo*, reflecting a limitation of our technique[50]. Therefore, it is possible that at the later timepoints, the MO was targeted for degradation, leading to reduced phenotypic effects. Second, continued differentiation of neural crest cells into neurons beyond E4-5 (HH24-27)[1] may be occurring and compensating for effects on placodal neurons after N-cadherin knockdown, and we would not be able to distinguish this based on Tubb3 immunostaining alone.

The placode contribution of the trigeminal ganglion is attributed to two distinct placodes, OpV and MmV, which express specific genes and undergo differentiation at different times[51,52]. In line with previous work[27], we observed more drastic phenotypes in OpV versus MmV trigeminal neurons. Although it is possible that N-cadherin is differentially required in the two placodes, we suspect this difference is most likely due to MO dilution over time in MmV. OpV placode cells are the first to express neuron-specific markers and adopt a post-mitotic neuronal fate, some even before leaving the ectoderm, which would lead to more discernable phenotypes given the timing of electroporation. Conversely, MmV placode cells remain as neuroblasts until after delamination[8–10] and continue to undergo cell division before differentiating into neurons and becoming post-mitotic. In the OpV lobe, E3.5 (HH19-22) showed the greatest difference in size. This time point represents when the majority of placodal neurons have initiated growth to their target tissues[24], therefore potentially explaining the more drastic phenotype at this stage. If N-cadherin promotes axon outgrowth, then its reduction could provide an explanation for the observed results.

Given these alterations to trigeminal ganglion morphology and the known absence of an effect on placode cell ingression after N-cadherin knockdown[27], we evaluated whether phenotypes were due to changes in the number of cells present within the trigeminal ganglion, including effects on the other critical cell population, the neural crest. This was particularly important to assess due

to the requirement for reciprocal interactions between placodal neurons and neural crest cells during trigeminal gangliogenesis[25], since disrupting a cadherin on one cell type could impact interactions with the other. Our results showed no change in the number of neural crest cells within the trigeminal ganglion nor an increase in apoptosis after N-cadherin knockdown. The TUNEL signal did not preferentially co-localize with MO-positive cells, and neural crest and placode cells appeared equally apoptotic. Therefore, apoptosis is not a driving factor behind the reduction in trigeminal ganglion size after N-cadherin knockdown. Moreover, the TUNEL signal preferentially localized adjacent to Sox10-positive nuclei, suggestive of glial phagocytosis as previously reported[53].

Reducing N-cadherin in placodal neurons impacts OpV nerve innervation patterns

Traveling away from the cell bodies housed in the trigeminal ganglion, we ascertained how N-cadherin knockdown in placodal neurons impacts OpV axon outgrowth to target tissues. We uncovered a differential requirement for N-cadherin in the lateral and medial nasal branches of OpV, with the former exhibiting more drastic changes upon N-cadherin MO treatment. We found decreases in axon number, nerve width, and innervation area in the lateral nasal nerve while the medial nasal nerve exhibited similar trends for nerve width and innervation area, albeit to a lesser extent. Interestingly, there was no change in the number of axons in the medial nasal branch. This contrasting result - a smaller nerve bundle having similar axonal branching - suggests that N-cadherin functions to adhere individual axons at targets to each other for the medial nasal branch. Similar phenotypes after N-cadherin perturbations have been observed in other systems as well[43,54,55].

Although both OpV branches begin developing at similar stages[45], we chose to examine the E5.5 (HH26-27) stage group for the medial nasal nerve studies due to more consistency among embryos. While possible that the difference in the age of embryos examined between the nerve branches could explain the varying results, we believe it is equally plausible that N-cadherin-expressing placodal neurons are required differently in the two branches. The contribution of neural crest- and placode-derived neurons has not been examined for these nerve branches, making it possible that neural crest- and placode-derived neurons comprise the bulk of the medial nasal and lateral nasal nerves, respectively. Additionally, the differences observed could be due to when the respective branches develop. Our results suggest that medial nasal branch development occurs after the lateral nasal branch. If true, then early knockdown of N-cadherin would preferentially impact the lateral nasal nerve since it develops first. Although most embryos had reduced nerve branch measurements, a subset showed increased nerve widths and innervation areas. This suggests that while the overt phenotype of N-cadherin knockdown leads to deficiencies in target

innervation by placodal neurons, a subset, potentially the earliest ones to extend axons, is still able to grow.

N-cadherin-mediated interactions facilitate the outgrowth of trigeminal neurons

To understand whether the phenotypes seen *in vivo* were due to an adhesion-dependent role of N-cadherin during trigeminal gangliogenesis, we utilized a function-blocking antibody to prevent N-cadherin-mediated adhesion. Multiple parameters, including antibody concentrations and incubation times, were tested to optimize conditions. Intriguingly, regardless of the incubation time prior to anti-N-cadherin treatment, some axon outgrowth occurred, suggesting that some trigeminal axons are dependent on N-cadherin for outgrowth, while others are not.

Analysis of the anti-N-cadherin *in vitro* experiments led to three major conclusions. First, overall, fewer trigeminal axons grew towards the periphery. Second, our intersection analyses indicated reduced axon outgrowth and branching when N-cadherin adhesion is abrogated. Lastly, no significant differences were noted in the average segment length, used as a proxy for axons, when comparing controls to anti-N-cadherin-treated explants. This indicates that the subset of trigeminal neurons unaffected by blocking N-cadherin function can reach the periphery in the same manner as their control counterparts, suggesting N-cadherin is not important for the outgrowth of these neurons. This conclusion models what was observed *in vivo* when examining OpV target innervation. In both instances, N-cadherin knockdown did not completely inhibit target innervation but instead reduced the number of axons successfully reaching target tissues. While this phenotype could be attributed to the mosaic nature of the MO electroporation, our *in vitro* results now offer another explanation, in that some neurons are not reliant on N-cadherin for the outgrowth of their axons.

Trigeminal neurons that do not rely on N-cadherin adhesion for axon outgrowth are of placodal origin and could represent a subpopulation of pioneer neurons

Given the timeline associated with trigeminal neuron differentiation from placode and neural crest cells *in vivo*[12], we speculated that this would be maintained in trigeminal explants and that we might see similar results to our *in vivo* data after blocking N-cadherin function *in vitro*. Our experiments showed reduced axon outgrowth in anti-N-cadherin-treated explants possessing RFP-labeled placodal neurons, recapitulating results from the anti-N-cadherin wildtype explant experiments and our observations *in vivo*. Although total levels of RFP were unchanged between treatments, very interestingly, the distribution of RFP observed within explants versus in extended axons was altered after treatment with the anti-N-cadherin antibody. Decreased RFP was detected in axonal projections after anti-N-cadherin-treatment, with the majority of RFP signal coming from inside the explanted tissue. This indicates that N-cadherin promotes axon outgrowth, with its absence limiting the amount of RFP-positive placodal neurons capable of extending axons from

the explanted tissue. Surprisingly, a small subset of RFP-positive placodal neurons exhibited axon outgrowth after anti-N-cadherin treatment, indicating that not all placodal neurons rely on N-cadherin in the same manner for axonal outgrowth.

When considering which molecules this subpopulation of placodal neurons rely for outgrowth, there are many possibilities including other cadherins and/or other guidance molecules such as Semaphorins, Ephrins, Netrins, and Robo/Slit[56]. However, it is unlikely that the typical axon guidance molecules would be available *in vitro* in the same manner as they would be *in vivo* since they are absent in the culture media. Instead, this subset of neurons appears to interact more intricately with their surrounding environment than they do with other trigeminal neurons to facilitate their outgrowth. In this study, slides were coated with the extracellular matrix protein fibronectin, making it the sole ligand available to which neurons can adhere. Integrins, a main receptor for fibronectin, are necessary for proper neurodevelopment[57] and may be utilized by this subpopulation of placodal neurons for their outgrowth. Alternatively, mesenchymal cells that were inadvertently included during dissection could promote the outgrowth of this neuronal subpopulation. Although it is possible these neurons could be engaging in N-cadherin-mediated adhesion with N-cadherin-expressing cranial mesenchyme[34] *in vivo*, sensory neurons prefer neural crest corridors over the mesoderm, as they are a more permissive substrate[58]. Additionally, this is not the case *in vitro* as all N-cadherin function was blocked with the use of the anti-N-cadherin antibody. Taken together, this subgroup of placodal neurons could be the true pioneers of the trigeminal ganglion, as they rely more heavily on guidance cues and interactions with their environment than they do on cell adhesion. In contrast, followers commonly utilize cell adhesion molecules to grow along axon tracts established by the pioneers[40]. To demonstrate this definitively, cell lineage tracing experiments, in which both neural crest and placode cells are labeled, are required to monitor their neuronal differentiation over developmental time, which is beyond the scope of this current study.

Reciprocal interactions between neural crest- and placode-derived trigeminal neurons are facilitated by N-cadherin and persist throughout trigeminal ganglion development

Our studies revealed that blocking the function of N-cadherin *in vitro* disrupts the normal axon outgrowth of placodal neurons. However, whether the axon outgrowth of neural crest-derived neurons is affected in a non-cell autonomous manner had not been explored. Fluorescent labeling of neural crest cells followed by reducing N-cadherin from placode cells with the N-cadherin MO revealed very few neural crest-derived axons (Supplemental Figure 3). Thus, neurites were evaluated, as they precede axon outgrowth[49]. We observed reduced neurite number and complexity after N-cadherin MO treatment, revealing non-cell autonomous effects on neural crest-derived neurons. These findings further highlight the continued importance of reciprocal

interactions throughout trigeminal gangliogenesis, now between placode- and neural crest-derived neurons.

N-cadherin functions in the production of neurites for other peripheral neurons[36], and its concentrated localization at specific sites along the cell membrane precedes neurite formation[59]. Depletion of N-cadherin from placodal neurons could disrupts *trans* N-cadherin interactions between neural crest cells/neural crest-derived neurons and placodal neurons, subsequently impacting N-cadherin expression on the membrane of neural crest-derived neurons and perturbing neurite production. Additionally, N-cadherin is involved in the maintenance of dendrites[43], leading to the possibility that neural crest-derived neurites are less stable and retract more quickly upon N-cadherin knockdown in placodal neurons. Irrespective of the mechanism behind reduced neurite formation, it is likely that disruptions to the cytoskeleton play a role. Membrane-bound N-cadherin regulates the availability of both β-catenin and p120-catenin for binding and activating various signaling pathways[60]. If less N-cadherin is present on the plasma membrane of neural crest-derived neurons, the typical intracellular signaling required to activate GTPases and other cytoskeletal remodeling proteins could be lost, leading to disruptions in neurite production.

GFP-positive neural crest-derived neurons in N-cadherin MO-treated explants were far less prevalent compared to N-cadherin MM-treated explants. Additionally, GFP-positive puncta that often co-localized with DAPI-positive cellular debris were observed in N-cadherin MO-treated explants, raising the possibility of increased apoptosis of neural crest-derived neurons. Interactions between cadherins and receptor tyrosine kinases at cellular membranes reportedly regulate each other[61], including those occurring between N-cadherin and Fibroblast Growth Factor receptor[62,63], which may be critical for the proper growth, maturation, and survival of neural crest-derived neurons. If neural crest-derived neurons now possess less membrane-bound N-cadherin due to N-cadherin depletion from placodal neurons, this could abrogate any N-cadherin-growth factor receptor interactions and lead to aberrant apoptosis of neural crest-derived neurons, in line with the punctate GFP observed in MO-treated explants. Further experimentation is needed to confirm this possibility.

Although fewer neurites were observed in N-cadherin MO-treated explants, neurite length did not differ from N-cadherin MM-treated explants. This finding could indicate that like placodal neurons, there is a subset of neural crest-derived neurons that do not require N-cadherin for axon outgrowth. The labeling of neural crest cells with a fluorescent reporter, followed by treating explants with the anti-N-cadherin antibody and tracking axon outgrowth, would aid in answering this question.

Conclusion

In this study, we have shown a sustained negative impact on the trigeminal ganglion after N-cadherin is depleted from placodal neurons. Changes to the size of the trigeminal ganglion, as well as reduced axon outgrowth to target tissues, are observed at early stages of development as well as later stages when neural crest cells have differentiated into neurons. These morphological differences cannot be explained by increased apoptosis or decreased neural crest cell number, suggesting an issue with the ability of neurons to properly extend axons in the absence of N-cadherin. Blocking the extracellular domain of N-cadherin, which abrogates adhesion, reduces axon outgrowth, recapitulating results seen *in vivo*. Furthermore, depleting N-cadherin from placodal neurons alters neurite production in neural crest-derived neurons in a non-cell autonomous manner, adding to the growing amount of research supporting the importance of reciprocal interactions between these two cell types during the formation of the cranial ganglia. Collectively, our results highlight a long-term, critical role for N-cadherin during trigeminal gangliogenesis.

Materials and Methods

Chick embryos

Fertilized chicken eggs (*Gallus gallus*) were obtained from the Department of Animal and Avian Sciences at the University of Maryland (MD) and Centurion Poultry Incorporated (GA) and incubated at 37°C in humidified incubators on their sides. Embryos were incubated to reach desired Hamburger Hamilton (HH) stages based on times provided therein[64]. Embryos were staged with this method or by counting the number of somite pairs (somite stage, ss).

Morpholinos

To reduce N-cadherin protein expression, a validated lissamine-tagged translation-blocking morpholino antisense oligonucleotide (MO) against *N-cadherin* was used (GeneTools, LLC)[27], with a sequence of 5'-GCGGCGTTCCCGCTATCCGGCACAT-3'. For control experiments, a 5 base pair mismatch N-cadherin control MO (N-cadherin MM) was used[27], with a sequence of 5'-GCGcCcTTCCCcCTATgCcGCACAT-3' (altered base pairs in lowercase). Both MOs were diluted with ultrapure water and 10% sucrose (in 1X phosphate-buffered saline (PBS)) and used at a final concentration of 500 μM.

In ovo unilateral placode electroporation

To target trigeminal placode cells prior to their delamination, a unilateral electroporation was performed at E1.75 (HH10-11). The N-cadherin MO, N-cadherin MM, or a combination of PiggyBacRFP, a genome incorporating vector[65] (0.819 μg/μl), with PBase, its transposase (0.912 μg/μl), was expelled on top of the ectoderm on one side of the embryo using a fine glass needle. Next, a 30-gauge needle was used to puncture a small hole through the vitelline membrane so that electrodes could lay vertically above and below the ectoderm over which the MO/plasmid had been placed. Three, 9V pulses were delivered over 50 ms at 200 ms intervals. After electroporation, eggs were resealed with tape and parafilm and grown at 37°C to desired stages of interest. Due to the inherent variations that arise during normal development, even when embryos are staged identically, the contralateral side of the electroporated embryo was a more appropriate control and was used for all *in vivo* studies. Initial experiments comparing N-cadherin MO-electroporated embryos to N-cadherin MM-electroporated embryos were conducted to ensure none of the reported phenotypes was due to the electroporation method (see Supplemental Figure 1). These results revealed that the trigeminal ganglia of N-cadherin MM-electroporated embryos developed in a similar manner to the contralateral control trigeminal ganglia observed in these and N-cadherin MO-treated embryos. All embryos were screened for successful MO electroporation based on the red fluorescence of the MO prior to collection and use in subsequent assays.

Sequential electroporation method

To target both cell populations that contribute to the trigeminal ganglion, a modified sequential electroporation[26] was utilized. Briefly, a unilateral neural tube co-electroporation was first performed on E1.5 (HH9) using a combination of PiggyBacGFP (0.819 µg/µl) and PBase[66] (0.912 µg/µl). Two 15V pulses were delivered over 30 ms at 200 ms intervals. The electroporated embryos were re-incubated until they reached E1.75 (HH10-11), and then the placode cells on the same side of the embryo were electroporated with the N-cadherin MO or N-cadherin MM in the same manner as described above. After this second electroporation, eggs were resealed with tape and parafilm and grown at 37°C to desired stages of interest.

Immunostaining

Electroporated embryos were collected at desired stages of interest and fixed in 4% paraformaldehyde (PFA) overnight at 4°C with agitation. Following fixation, embryos were washed 3 x 10 minutes in 1X PBS and stored in 1X PBS at 4°C until further processing. Primary antibodies used included Tubb3 (Abcam ab78078, 1:500 for section, 1:250 for whole-mount), Sox10 (GeneTex GTX128374, 1:250), GFP (Abcam ab6662, 1:250), and RFP (Invitrogen MA5-15257, (1:250). Secondary antibodies used included goat anti-rabbit 405 (ThermoFisher), goat anti-mouse IgG_1 594 (Invitrogen), and goat anti-mouse IgG_{2a} 555 or 647 (SouthernBiotech).

Tissue sections: Embryos were processed through an increasing sucrose gradient (5% and 15% sucrose (Fisher) in 1X PBS) at 4°C either overnight or until they sank to the bottom of the vials. Next, they were processed through 7.5% gelatin (Sigma) in 15% sucrose and 20% gelatin in 1X PBS, both at 37°C, either overnight or until the embryos sank. Embryos were embedded in 20% gelatin, flash-frozen using liquid nitrogen, and stored at -80°C until ready for use. Embedded embryos were then cryo-sectioned at 12 µm on charged slides (VWR). Slide-mounted tissue sections were stored at -20°C until ready for use. For immunohistochemistry, slides were de-gelatinized by incubation in 1X PBS at 42°C for 15-20 minutes. Following 3 x 5-minute washes in 1X PBS, the slides were blocked with 10% heat-treated sheep serum (Sigma, HTSS) in PBST (Sigma, 1X PBS + 0.1% Triton X-100) at room temperature for 1-2 hours in a humidified chamber, then rinsed in PBST. Primary antibodies were diluted in PBST + 5% HTSS, added to the slides, covered with a glass coverslip (Fisher) to prevent sections from drying out, and incubated overnight at 4°C. The following day, the coverslips were removed, and the slides were washed 4 x 30 minutes in PBST. Secondary antibodies were then diluted in PBST + 5% HTSS, added to the slides, covered with a glass coverslip, and incubated overnight at 4°C. The next day, slides were again washed 4 x 30 minutes in PBST and mounted with DAPI-fluoromount media (SouthernBiotech).

Standard whole-mount immunohistochemistry: Embryos were blocked with 10% HTSS in PBST for 2 hours at room temperature. Following a rinse with PBST, primary antibodies were

diluted in PBST + 5% HTSS and incubated overnight at 4°C with agitation. The following day, the embryos were washed 4 x 30 minutes in PBST. Secondary antibodies were diluted in PBST + 5% HTSS and incubated overnight at 4°C with agitation. The next day, embryos were again washed 4 x 30 minutes in PBST and stored in 1X PBS at 4°C until they were either imaged or FRUIT cleared (see below).

Modified whole-mount immunohistochemistry for iDISCO clearing: An adapted protocol was used based on methods from[67]. Fixed embryos were washed 2 times for 1 hour in 1X PBS and then were taken through an increasing methanol (MeOH, Pharmco in 1X PBS) gradient (50% (1 x 1 hour), 80% (1 x 1 hour), 100% (2 x 1 hour)), before they were bleached overnight in 5% H_2O_2 (Sigma) in 20% DMSO (Fisher)/methanol at 4°C. The next day, samples were taken through the following series of washes: 2 x 1 hour in 100% MeOH, 2 x 1 hour in 20% DMSO/MeOH, 1 x 1 hour in 80% MeOH, 1 x 1 hour in 50% MeOH, 2 x 1 hour in 1X PBS, and 2 x 1 hour in 1X PBS + 0.2% Triton X-100. Samples were incubated overnight in 20% DMSO/0.3M glycine (Fisher) in 1X PBS + 0.2% Triton X-100 at 4°C. The next day, samples were blocked in 10% HTSS/10% DMSO/1X PBS + 0.2% Triton X-100 overnight at 4°C. Embryos were washed 2 x 1 hour in 0.2% Tween-20 (Sigma) in 1X PBS with 10 µg/ml heparin (Fisher, PTwH) at room temperature before primary antibodies were added and incubated for 72 hours at 4°C. Primary antibodies were diluted in 5% DMSO/5% HTSS/PTwH. Samples were washed in PTwH for 24 hours before secondary antibodies were added (diluted in the same manner as the primary antibodies), and samples were incubated with secondary antibodies for 48 hours at 4°C. Samples were then washed for 48 hours in PTwH before iDISCO clearing (see below).

Explant immunocytochemistry: Explant slides were washed once with 1X PBS, followed by fixation in 4% PFA for 1 hour at room temperature with agitation. Following fixation, slides were rinsed with 1X PBS and stored in 1X PBS at 4°C until ready for immunocytochemistry. A hydrophobic perimeter was drawn around the slides to prevent dehydration of tissue using an ImmEdge Pen (Vector Laboratories), and explants were taken through blocking, primary antibody incubation, and secondary antibody incubation in the absence of coverslips as described in the tissue section methods. Slides were mounted with DAPI-fluoromount media (SouthernBiotech) and covered with a glass coverslip.

Tissue Clearing

As embryos progress through development and tissue structures surrounding the trigeminal ganglion become more complex, visualization of the trigeminal ganglion after whole-mount immunohistochemistry became increasingly difficult. Therefore, clearing methods to render the tissues transparent were performed. At early stages (up to E3.5, HH22), the FRUIT[68] tissue

clearing protocol was used, whereas later stages required iDISCO[67] tissue clearing. With both protocols, MO fluorescence was quenched during the clearing process.

FRUIT: Following the standard whole-mount immunohistochemistry protocol, embryos were progressed through increasing concentrations of fructose (35%, 40%, 60% and 80% w/v) in 8M urea (Sigma), 0.5% (v/v) alpha-thioglycerol (Fisher) dissolved in ultrapure water ("FRUIT buffer") for a minimum of 8 hours, up to 24 hours at room temperature, depending on the stage of the embryo. The time spent in a certain concentration of FRUIT buffer was determined based on how quickly the sample was rendered transparent. A sample was only moved up to the next FRUIT buffer once it had visibly changed transparency. The FRUIT cocktail, containing increasing concentrations of fructose, was made by first dissolving fructose in ultrapure water at 37°C. Once dissolved, the urea was added, and the solution was rocked at room temperature until fully dissolved. Lastly, alpha-thioglycerol was added, and buffers were stored at 4°C until use. Embryos were imaged in 60% or 80% FRUIT buffer (depending on the stage of the embryo) in glass-bottomed petri dishes (Mat-tek). Typically, embryos up to E3 (HH19) were imaged in 60% FRUIT while E3+ (HH20-22) staged embryos were imaged in 80% FRUIT.

iDISCO: Following the modified whole-mount immunohistochemistry protocol, embryos were washed in PBST (0.2%) for a minimum of 48 hours. Samples were incubated in 50% (v/v) tetrahydrofuran (THF, Sigma) in water overnight in glass vials, making sure that over 90% of the vial was filled with the solution. The following day, embryos were then incubated in 80% THF in water for one hour, followed by 2 x 1-hour incubations in 100% THF. Next, samples were incubated in 100% dichloromethane (Sigma) for 1-2 hours (or until they sank to the bottom of the vial). Lastly, embryos were incubated in dibenzyl ether (DBE, Sigma) overnight and imaged the following day in DBE. All of the previous steps were performed at room temperature, and embryos were also at room temperature in DBE. iDISCO-cleared embryos were imaged in a glass petri dish containing a custom chamber[67], which was printed in Terrapin Works, part of the School of Engineering at the University of Maryland.

TUNEL assay

To assess apoptosis, the *In Situ* Cell Death Detection Kit, Fluorescein (Roche) was used according to manufacturer's instructions. Briefly, following secondary antibody washes (4 x 30 minutes in PBST (0.1%)), slides were washed once for 30 minutes in 1X PBS. Slides were re-fixed with 4% PFA for 20 minutes at room temperature, followed by one 30-minute wash in 1X PBS. The TUNEL reaction mixture was added to the slides (75 µL per slide), and a glass coverslip was placed over them. Slides were incubated in the dark for 1 hour at 37°C. Next, the coverslips were removed, and the slides were washed 3 x 5 minutes in 1X PBS. Lastly, slides were mounted with DAPI-fluoromount media (SouthernBiotech).

Trigeminal ganglion explant assay

Wildtype E2 (HH13/14) embryos were removed from eggs and stored on ice in 1X PBS until dissections. Trigeminal ganglia were dissected on a sylgard-coated dish by first bisecting the embryo and then carefully taking the area of the forming trigeminal ganglion, making sure to exclude the eye and neural tube. Explants were cultured on 2-well glass chamber slides (ThermoFisher) coated with Poly-L-Lysine (0.01% PLL, Sigma) and fibronectin (0.01%, Sigma). To make the coated slides, PLL (diluted in ultrapure water) was added to each chamber on the glass slides and incubated inside a biosafety cabinet for 30 minutes at room temperature. The PLL was removed, and slides were washed 3 times with water. Next, fibronectin (diluted in DMEM media (ThermoFisher)) was added to each chamber and incubated at 37°C for a minimum of 2 hours. The fibronectin solution was removed, and slides were stored at 4°C until needed (for up to one week). Explants were grown in DMEM media supplemented with N2 (1%, ThermoFisher) and Penicillin/Streptomycin (1%, Fisher). Explants for N-cadherin function blocking antibody experiments (see below) were grown in the supplemented DMEM media mentioned above. Sequentially labeled cells for N-cadherin MO- or MM-containing explant experiments were grown in Neurobasal media (ThermoFisher) supplemented with B27 (1%, ThermoFisher), N2 (0.5%, ThermoFisher), Glutamax (1%, ThermoFisher), Penicillin/Streptomycin (1%, ThermoFisher), and with nerve growth factor (ThermoFisher), brain-derived neurotrophic factor (Amgen), and neurotrophin-3 (Amgen), all at 50 ng/ml.

N-cadherin function-blocking antibody experiments

After 24 hours of incubation, fresh media containing either an antibody to block N-cadherin function, MNCD2 (anti-N-cadherin, Developmental Studies Hybridoma Bank, 0.1 µg/ml), or a normal rat IgG control (Santa Cruz Biotechnology, 1.6 µg/ml), replaced the initial explant plating media and explants were incubated overnight. The following morning, the slides were briefly rinsed with 1X PBS, and then fixed in 4% PFA for one hour at room temperature. The explants were washed 3 times in 1X PBS, and then processed for immunocytochemistry.

Confocal imaging

All images were acquired with the LSM Zeiss 800 confocal microscope (Carl Zeiss Microscopy, Thornwood, NY, USA). Laser power, gain, and offset were kept consistent for the different channels during all experiments where possible. Fiji (NIH)[69] and Adobe Photoshop CC 2023 were used for image processing. For whole-mount imaging with Z-stacks, all embryos were imaged at a 5 µm interval. For sections, images of at least five serial transverse sections were acquired and used for analysis. For all experiments, a minimum of five replicates was obtained.

Quantifications and statistical analyses

Surface area: For modified surface area measurements of the whole trigeminal ganglion, the OpV lobe, and the MmV lobes, maximum intensity Z-projections were first generated from Z-stacks taken through the trigeminal ganglion using Fiji. The polygon tool was used to outline the perimeter of Tubb3 signal and area measurements were generated. Individual area measurements for each developmental stage grouping were averaged together and plotted to generate graphs in PRISM (GraphPad Software, Inc.)

Sox10- and TUNEL-positive cell counting: N-cadherin MO-treated embryos were processed for section immunohistochemistry for Sox10 and Tubb3, followed by the TUNEL staining protocol. Once imaged, the individual channels were opened on Fiji. With the Tubb3 channel image, the polygon tool was used to trace the outline of the trigeminal ganglion. The outline was added to the region of interest manager, and then used to crop both the TUNEL channel and Sox10 channel to only include the area of the image that contained neurons of the trigeminal ganglion. Once images from all experiments were processed, they were analyzed using the Squassh[70] plugin from the MOSAICsuite[71] in Fiji, as described[26]. Segmentation parameters were kept uniform for all images in one experimental condition (Sox10 or TUNEL) and run as a batch function. Following batch analysis, the quality of image segmentation was confirmed visually to ensure accurate segmentation. If batch parameters were not sufficient, they were adjusted on a case-by-case basis and the segmentation analysis was rerun. For TUNEL analysis, the number of puncta (observed as objects) was calculated per image and averaged to obtain an average number per replicate. Individual averages for each developmental stage grouping were averaged together and plotted to generate graphs. For Sox10 nuclei counting, a further adjustment was made to accurately account for all nuclei in an image. After the segmentation was run, two values were found: the median area of nuclear objects and the total area of all objects. The total area was divided by the median nuclei size to generate an adjusted nuclei count. The adjusted count was found per image and averaged to obtain an average number per replicate. Individual averages for each developmental stage grouping were averaged together and plotted to generate graphs.

Nerve branching: Z-stack images of the OpV branch of the trigeminal nerve were analyzed in Fiji using custom ImageJ Macro language (IJM) scripts (available upon request). Maximum intensity Z-projection images were generated and inputted into the ImageJ macro. Signal profiles were obtained via successive vertical line selections using *getProfile()* at 30 μm intervals. The number of individual axons present at increasing distances from the starting point were exported and calculated in R (R core team, Vienna, Austria, 2021, scripts available upon request). Data for individual replicates for each condition were aligned so that quantification of nerve branching over a distance concordantly began with the first measurement found. Data were displayed as the mean quantity of nerve branches and plotted to generate graphs.

Nerve width: Using maximum intensity Z-projections, nerve width measurements for both the lateral and medial nasal nerves were generated using the straight line tool on Fiji. The width of individual OpV nerve divisions (prior to the point of extensive branching within the target tissue) was measured based on Tubb3 signal for each embryo. Widths were averaged for N-cadherin MO-treated embryos and their contralateral control sides and plotted to generate graphs.

Innervation area: Using maximum intensity Z-projections, innervation area measurements for both the lateral and medial nasal nerves were generated using the polygon tool on Fiji. A border was drawn around the Tubb3 signal in respective target tissues where terminal nerve branching occurred. Individual area measurements were averaged together for N-cadherin MO-treated embryos and their contralateral control sides, then plotted to generate graphs.

Intersection analysis following treatment with anti-N-cadherin: Each low magnification (5X), tiled image of the explants was imported into Fiji. Background was removed and the ridge-detection plug-in[72] was used to highlight axonal outgrowth to quantify axon length. Using the detected segment binary images and the concentric circle plugin, 20 concentric circles were overlayed on the explant, centered at the middle of the explant. The number of axonal intersections at each successive ring of increasing diameter was counted and plotted as mean ± SEM at 175 μm intervals.

RFP-labeled placode cell analysis: Each low magnification (5X), tiled image of the Tubb3 channel was first inputted into Fiji and background was eliminated. A polygon selection feature was used to isolate the main body of the explant from its associated axonal projections. The fluorescent intensity of RFP signal was collected for both the axonal projections and the body of the explant. The mean signal of each was compared to the total signal for the entire explant, averaged across treatments, and compared between conditions.

Simple neurite tracer analysis: Each high magnification (40X) Z-stack of GFP-positive neural crest-derived neurons was opened on Fiji using the simple neurite tracer plugin[73,74]. Starting from the cell body, primary neurites were traced as paths. Neurites extending from primary neurites were added as branch points and termed secondary neurites. Any neurite branching off secondary neurites was marked as a tertiary neurite. The number of neurites per soma, as well as the length of individual neurites, was compiled into a spreadsheet where mean neurite number and mean neurite length of primary, secondary, and tertiary neurites were plotted as scatterplots.

Acknowledgments

The authors would like to thank the National Institute of Dental and Craniofacial Research (R01DE024217) and the University of Maryland Graduate School for financially supporting this research. Additionally, we would like to thank Ms. Zoe Davidson and Ms. Reagan Armstrong for their technical assistance. All schematics were created with Biorender.com.

References

1. D'Amico-Martel, A. & Noden, D. M. An autoradiographic analysis of the development of the chick trigeminal ganglion. *J Embryol Exp Morphol* **55**, 167–182 (1980).
2. Hamburger, V. Experimental analysis of the dual origin of the trigeminal ganglion in the chick embryo. *J. Exp. Zool.* **148**, 91–123 (1961).
3. Noden, D. M. The migratory behavior of neural crest cells. *Symp Oral Sens Percept* 9–36 (1973).
4. Lumsden, A., Sprawson, N. & Graham, A. Segmental origin and migration of neural crest cells in the hindbrain region of the chick embryo. *Development* **113**, 1281–1291 (1991).
5. Rodrigues-Da-Silva, M. A., De Espindola Da Silveira, G., Taufer, C. R. & Calloni, G. W. The mesenchymal potential of trunk neural crest cells. *Int. J. Dev. Biol.* **66**, 317–331 (2022).
6. Bronner, M. E. & LeDouarin, N. M. Development and evolution of the neural crest: An overview. *Developmental Biology* **366**, 2–9 (2012).
7. Bellairs, R. & Osmond, M. *The Atlas of Chick Development*. (Elsevier/AP, Academic Press is an imprint of Elsevier, Amsterdam, 2014).
8. Graham, A. & Shimeld, S. M. The origin and evolution of the ectodermal placodes. *Journal of Anatomy* **222**, 32–40 (2013).
9. Begbie, J. Early Steps in the Production of Sensory Neurons by the Neurogenic Placodes. *Molecular and Cellular Neuroscience* **21**, 502–511 (2002).
10. McCabe, K. L., Sechrist, J. W. & Bronner-Fraser, M. Birth of ophthalmic trigeminal neurons initiates early in the placodal ectoderm. *J of Comparative Neurology* **514**, 161–173 (2009).
11. Shiau, C. E., Das, R. M. & Storey, K. G. An effective assay for high cellular resolution time-lapse imaging of sensory placode formation and morphogenesis. *BMC Neurosci* **12**, 37 (2011).
12. D'Amico-Martel, A. & Noden, D. M. Contributions of placodal and neural crest cells to avian cranial peripheral ganglia. *Am. J. Anat.* **166**, 445–468 (1983).
13. Moody, S. A. & Heaton, M. B. Developmental relationships between trigeminal ganglia and trigeminal motoneurons in chick embryos. I. Ganglion development is necessary for motoneuron migration. *J of Comparative Neurology* **213**, 327–343 (1983).
14. Shiau, C. E., Lwigale, P. Y., Das, R. M., Wilson, S. A. & Bronner-Fraser, M. Robo2-Slit1 dependent cell-cell interactions mediate assembly of the trigeminal ganglion. *Nat Neurosci* **11**, 269–276 (2008).
15. Bate, C. M. Pioneer neurones in an insect embryo. *Nature* **260**, 54–56 (1976).
16. Klose, M. & Bentley, D. Transient pioneer neurons are essential for formation of an embryonic peripheral nerve. *Science* **245**, 982–984 (1989).

17. Lin, D. M., Auld, V. J. & Goodman, C. S. Targeted neuronal cell ablation in the drosophila embryo: Pathfinding by follower growth cones in the absence of pioneers. *Neuron* **14**, 707–715 (1995).
18. Hidalgo, A. & Brand, A. H. Targeted neuronal ablation: the role of pioneer neurons in guidance and fasciculation in the CNS of *Drosophila*. *Development* **124**, 3253–3262 (1997).
19. Clarke, A. *et al.* Dynamic morphogenesis of a pioneer axon in *Drosophila* and its regulation by Abl tyrosine kinase. *MBoC* **31**, 452–465 (2020).
20. Eisen, J. S., Myers, P. Z. & Westerfield, M. Pathway selection by growth cones of identified motoneurones in live zebra fish embryos. *Nature* **320**, 269–271 (1986).
21. Ghosh, A., Antonini, A., McConnell, S. K. & Shatz, C. J. Requirement for subplate neurons in the formation of thalamocortical connections. *Nature* **347**, 179–181 (1990).
22. Gong, Q. & Shipley, M. T. Evidence that pioneer olfactory axons regulate telencephalon cell cycle kinetics to induce the formation of the olfactory bulb. *Neuron* **14**, 91–101 (1995).
23. Stainier, D. Y. & Gilbert, W. Pioneer neurons in the mouse trigeminal sensory system. *Proc Natl Acad Sci U S A* **87**, 923–927 (1990).
24. Moody, S. A., Quigg, M. S. & Frankfurter, A. Development of the peripheral trigeminal system in the chick revealed by an isotype-specific anti-beta-tubulin monoclonal antibody. *J of Comparative Neurology* **279**, 567–580 (1989).
25. Steventon, B., Mayor, R. & Streit, A. Neural crest and placode interaction during the development of the cranial sensory system. *Developmental Biology* **389**, 28–38 (2014).
26. Halmi, C. A., Wu, C.-Y. & Taneyhill, L. A. Neural crest cell-placodal neuron interactions are mediated by Cadherin-7 and N-cadherin during early chick trigeminal ganglion assembly. *F1000Res* **11**, 741 (2022).
27. Shiau, C. E. & Bronner-Fraser, M. N-cadherin acts in concert with Slit1-Robo2 signaling in regulating aggregation of placode-derived cranial sensory neurons. *Development* **136**, 4155–4164 (2009).
28. Wu, C. & Taneyhill, L. A. Cadherin-7 mediates proper neural crest cell–placodal neuron interactions during trigeminal ganglion assembly. *genesis* **57**, e23264 (2019).
29. Straub, B. K. *et al.* E–N-cadherin heterodimers define novel adherens junctions connecting endoderm-derived cells. *The Journal of Cell Biology* **195**, 873–887 (2011).
30. Basu, R. *et al.* Heterophilic Type II Cadherins Are Required for High-Magnitude Synaptic Potentiation in the Hippocampus. *Neuron* **96**, 160-176.e8 (2017).
31. Niessen, C. M., Leckband, D. & Yap, A. S. Tissue organization by cadherin adhesion molecules: dynamic molecular and cellular mechanisms of morphogenetic regulation. *Physiol Rev* **91**, 691–731 (2011).

32. Hatta, K. & Takeichi, M. Expression of N-cadherin adhesion molecules associated with early morphogenetic events in chick development. *Nature* **320**, 447–449 (1986).
33. Nakagawa, S. & Takeichi, M. N-cadherin is crucial for heart formation in the chick embryo. *Dev Growth Differ* **39**, 451–455 (1997).
34. Dady, A., Blavet, C. & Duband, J.-L. Timing and kinetics of E- to N-cadherin switch during neurulation in the avian embryo. *Dev. Dyn.* **241**, 1333–1349 (2012).
35. Shiau, C. E. & Bronner-Fraser, M. N-cadherin acts in concert with Slit1-Robo2 signaling in regulating aggregation of placode-derived cranial sensory neurons. *Development* **136**, 4155–4164 (2009).
36. Bixby, J. L. & Zhang, R. Purified N-cadherin is a potent substrate for the rapid induction of neurite outgrowth. *J Cell Biol* **110**, 1253–1260 (1990).
37. Riehl, R. *et al.* Cadherin Function Is Required for Axon Outgrowth in Retinal Ganglion Cells In Vivo. *Neuron* **17**, 837–848 (1996).
38. Masai, I. *et al.* N-cadherin mediates retinal lamination, maintenance of forebrain compartments and patterning of retinal neurites. *Development* **130**, 2479–2494 (2003).
39. Benson, D. L. & Tanaka, H. N-Cadherin Redistribution during Synaptogenesis in Hippocampal Neurons. *J. Neurosci.* **18**, 6892–6904 (1998).
40. Jontes, J. D. The Cadherin Superfamily in Neural Circuit Assembly. *Cold Spring Harb Perspect Biol* **10**, a029306 (2018).
41. Itoh, K., Ozaki, M., Stevens, B. & Fields, R. D. Activity-dependent regulation of N-cadherin in DRG neurons: differential regulation of N-cadherin, NCAM, and L1 by distinct patterns of action potentials. *J Neurobiol* **33**, 735–748 (1997).
42. Inuzuka, H., Redies, C. & Takeichi, M. Differential expression of R- and N-cadherin in neural and mesodermal tissues during early chicken development. *Development* **113**, 959–967 (1991).
43. Tan, Z.-J., Peng, Y., Song, H.-L., Zheng, J.-J. & Yu, X. N-cadherin-dependent neuron–neuron interaction is required for the maintenance of activity-induced dendrite growth. *Proc. Natl. Acad. Sci. U.S.A.* **107**, 9873–9878 (2010).
44. Redies, C., Inuzuka, H. & Takeichi, M. Restricted expression of N- and R-cadherin on neurites of the developing chicken CNS. *J Neurosci* **12**, 3525–3534 (1992).
45. Higashiyama, H. & Kuratani, S. On the maxillary nerve: The Maxillary Nerve in Vertebrates. *Journal of Morphology* **275**, 17–38 (2014).
46. Bronner-Fraser, M., Wolf, J. J. & Murray, B. A. Effects of antibodies against N-cadherin and N-CAM on the cranial neural crest and neural tube. *Developmental Biology* **153**, 291–301 (1992).

47. Lu, Y., Lin, C. & Wang, X. PiggyBac transgenic strategies in the developing chicken spinal cord. *Nucleic Acids Research* **37**, e141–e141 (2009).
48. Macdonald, J. *et al.* Efficient genetic modification and germ-line transmission of primordial germ cells using piggyBac and Tol2 transposons. *Proc. Natl. Acad. Sci. U.S.A.* **109**, (2012).
49. Sainath, R. & Gallo, G. Cytoskeletal and signaling mechanisms of neurite formation. *Cell Tissue Res* **359**, 267–278 (2015).
50. Bill, B. R., Petzold, A. M., Clark, K. J., Schimmenti, L. A. & Ekker, S. C. A Primer for Morpholino Use in Zebrafish. *Zebrafish* **6**, 69–77 (2009).
51. Stark, M. R., Sechrist, J., Bronner-Fraser, M. & Marcelle, C. Neural tube-ectoderm interactions are required for trigeminal placode formation. *Development* **124**, 4287–4295 (1997).
52. Lassiter, R. N. T., Stark, M. R., Zhao, T. & Zhou, C. J. Signaling mechanisms controlling cranial placode neurogenesis and delamination. *Developmental Biology* **389**, 39–49 (2014).
53. Wu, H.-H. *et al.* Glial precursors clear sensory neuron corpses during development via Jedi-1, an engulfment receptor. *Nat Neurosci* **12**, 1534–1541 (2009).
54. Reis, S. A. *et al.* Striatal neurons expressing full-length mutant huntingtin exhibit decreased N-cadherin and altered neuritogenesis. *Human Molecular Genetics* **20**, 2344–2355 (2011).
55. Shikanai, M. *et al.* Caveolin-1 Promotes Early Neuronal Maturation via Caveolae-Independent Trafficking of N-Cadherin and L1. *iScience* **7**, 53–67 (2018).
56. Chilton, J. K. Molecular mechanisms of axon guidance. *Developmental Biology* **292**, 13–24 (2006).
57. Lilja, J. & Ivaska, J. Integrin activity in neuronal connectivity. *Journal of Cell Science* **131**, jcs212803 (2018).
58. Freter, S., Fleenor, S. J., Freter, R., Liu, K. J. & Begbie, J. Cranial neural crest cells form corridors prefiguring sensory neuroblast migration. *Development* **140**, 3595–3600 (2013).
59. Gärtner, A. *et al.* N-cadherin specifies first asymmetry in developing neurons. *EMBO J* **31**, 1893–1903 (2012).
60. Radice, G. L. N-Cadherin-Mediated Adhesion and Signaling from Development to Disease. in *Progress in Molecular Biology and Translational Science* vol. 116 263–289 (Elsevier, 2013).
61. Chiasson-MacKenzie, C. & McClatchey, A. I. Cell–Cell Contact and Receptor Tyrosine Kinase Signaling. *Cold Spring Harb Perspect Biol* **10**, a029215 (2018).
62. Nguyen, T. & Mège, R. M. N-Cadherin and Fibroblast Growth Factor Receptors crosstalk in the control of developmental and cancer cell migrations. *European Journal of Cell Biology* **95**, 415–426 (2016).

63. Hansen, S. M., Berezin, V. & Bock, E. Signaling mechanisms of neurite outgrowth induced by the cell adhesion molecules NCAM and N-Cadherin. *Cell. Mol. Life Sci.* **65**, 3809–3821 (2008).
64. Hamburger, V. & Hamilton, H. L. A series of normal stages in the development of the chick embryo. *Developmental Dynamics* **195**, 231–272 (1992).
65. Chen, F. & LoTurco, J. A method for stable transgenesis of radial glia lineage in rat neocortex by piggyBac mediated transposition. *J Neurosci Methods* **207**, 172–180 (2012).
66. Wang, W. *et al.* Chromosomal transposition of *PiggyBac* in mouse embryonic stem cells. *Proc. Natl. Acad. Sci. U.S.A.* **105**, 9290–9295 (2008).
67. Renier, N. *et al.* iDISCO: A Simple, Rapid Method to Immunolabel Large Tissue Samples for Volume Imaging. *Cell* **159**, 896–910 (2014).
68. Hou, B. *et al.* Scalable and DiI-compatible optical clearance of the mammalian brain. *Front Neuroanat* **9**, 19 (2015).
69. Schindelin, J. *et al.* Fiji: an open-source platform for biological-image analysis. *Nature Methods* **9**, 676–682 (2012).
70. Rizk, A. *et al.* Segmentation and quantification of subcellular structures in fluorescence microscopy images using Squassh. *Nat Protoc* **9**, 586–596 (2014).
71. Shivanandan, A., Radenovic, A. & Sbalzarini, I. F. MosaicIA: an ImageJ/Fiji plugin for spatial pattern and interaction analysis. *BMC Bioinformatics* **14**, 349 (2013).
72. Steger, C. An unbiased detector of curvilinear structures. *IEEE Trans. Pattern Anal. Machine Intell.* **20**, 113–125 (1998).
73. Arshadi, C., Günther, U., Eddison, M., Harrington, K. I. S. & Ferreira, T. A. SNT: a unifying toolbox for quantification of neuronal anatomy. *Nat Methods* **18**, 374–377 (2021).
74. Ferreira, T. A. *et al.* Neuronal morphometry directly from bitmap images. *Nat Methods* **11**, 982–984 (2014).

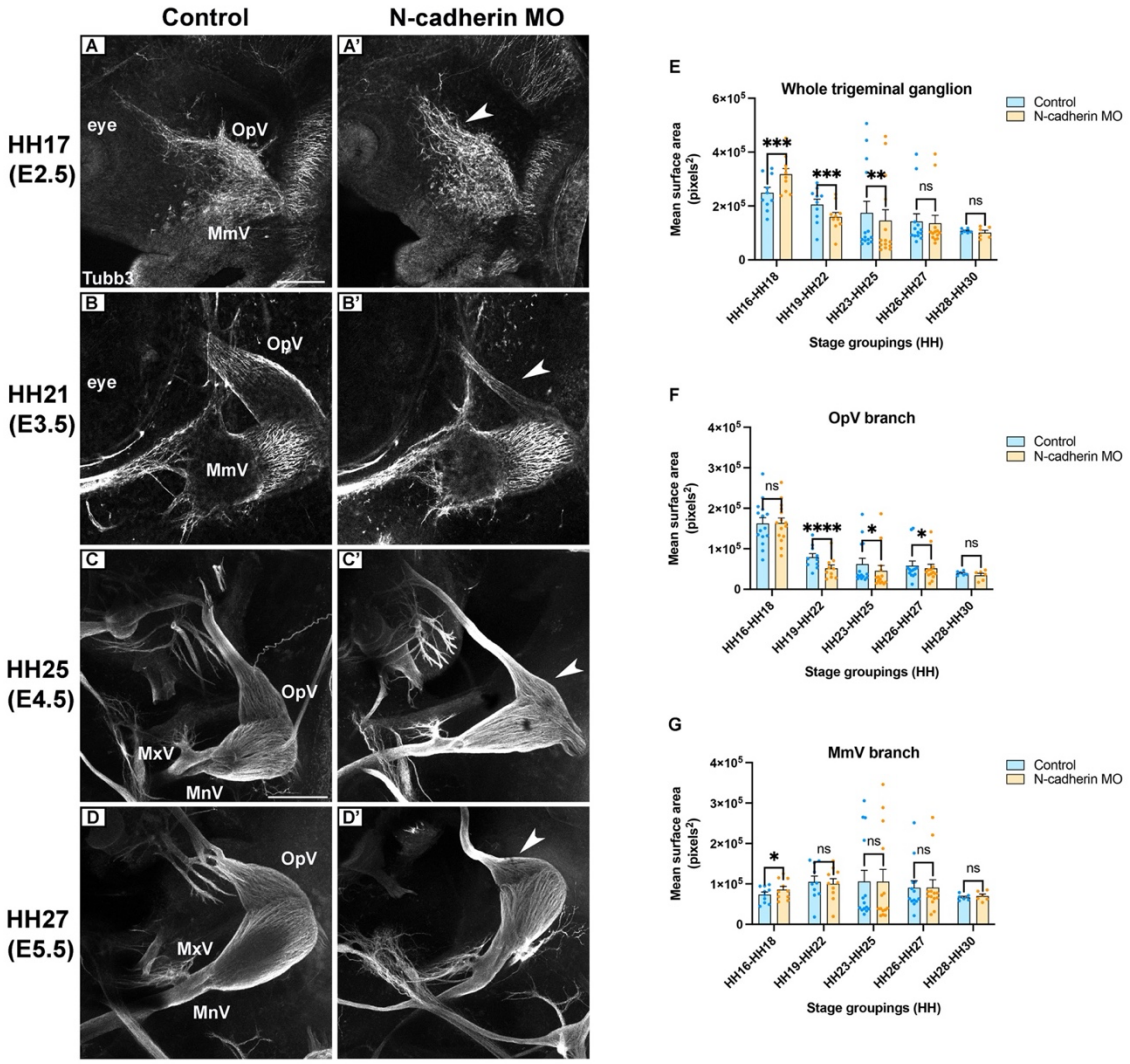

Figure 1. Knockdown of N-cadherin in placode cells disrupts trigeminal ganglion development. (A-D') Representative images of the trigeminal ganglion after immunostaining for Tubb3 and tissue clearing from various stage groupings (E2.5/HH16-18: A-A' (n=10), E3.5/HH19-22: B-B' (n=10), E4.5/HH23-25: C-C' (n=14), E5.5/HH26-27: D-D' (n=13), E6.5/HH28-30 (n=6)). Arrowheads highlight reductions in OpV lobe size in N-cadherin MO samples compared to controls. Scale bar in (A) is 250 µm and applies to (A'-B'). Scale bar in (C) is 250 µm and applies to (C'-D'). Mean whole trigeminal ganglia (E), OpV branch (F), and MmV/MxV branch (G) surface area ± SEM between contralateral and N-cadherin MO sides of embryos. Statistical significance was determined via paired t-tests. (*) $p<0.05$, (**) $p<0.01$, (***) $p<0.001$, (****) $p<0.0001$. Abbreviations: OpV: ophthalmic; MmV: maxillomandibular; MxV: maxillary; MnV: mandibular; ns: not significant.

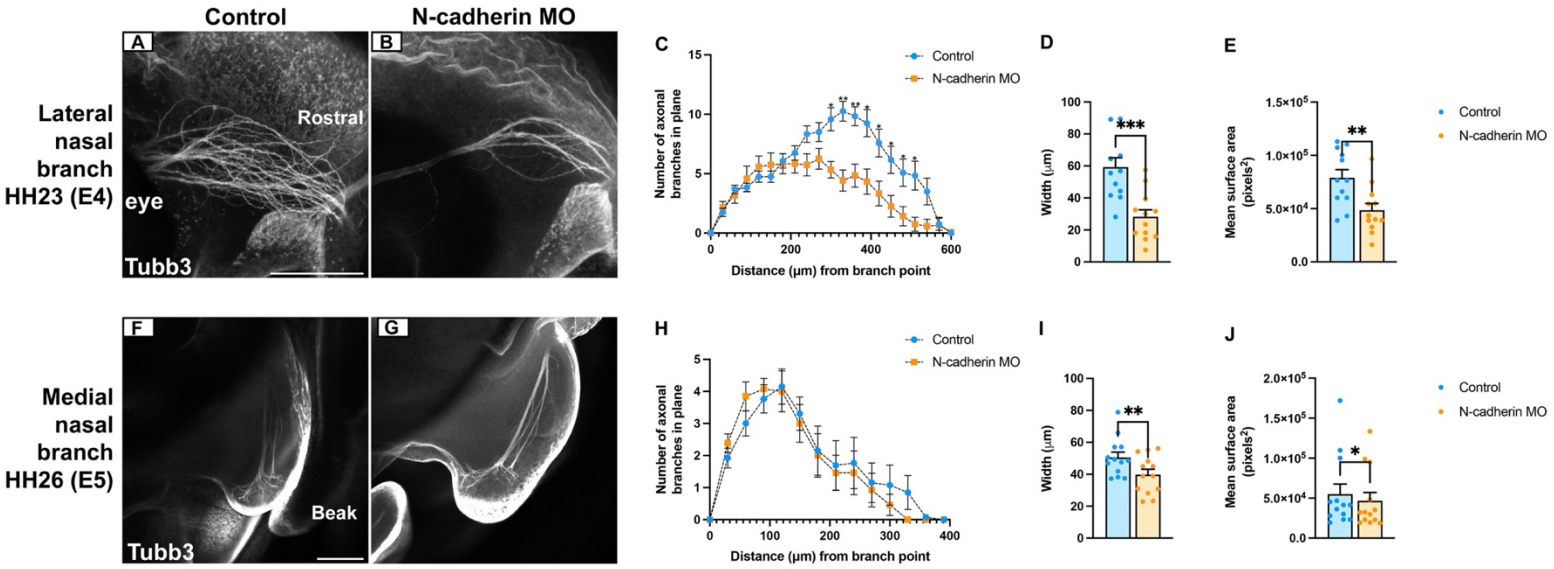

Figure 2. N-cadherin depletion from placode cells negatively impacts outgrowth and target tissue innervation for OpV nerve branches. (A, B, F, G) Representative images of the trigeminal ganglion following immunostaining for Tubb3 and clearing with iDISCO (A, B: E4.5/HH23-25, n=12; F, G: E5.5/HH26-27, n=13). Scale bars in (A) and (F) are 250 μm and apply to (B) and (G), respectively. (C, H) Mean ± SEM of axon branch counts at increasing distances from the trigeminal ganglion. (D, I) Mean nerve width ± SEM was calculated as a summation of the width of the nerve bundle prior to extensive axon branching. (E, J) Mean innervation area ± SEM was calculated by measuring the area where axons terminate. Statistical significance was determined via paired t-tests (C-E, H-J), with adjustments made for multiple comparisons (C, H). (*) $p<0.05$, (**) $p<0.01$, (***) $p<0.001$.

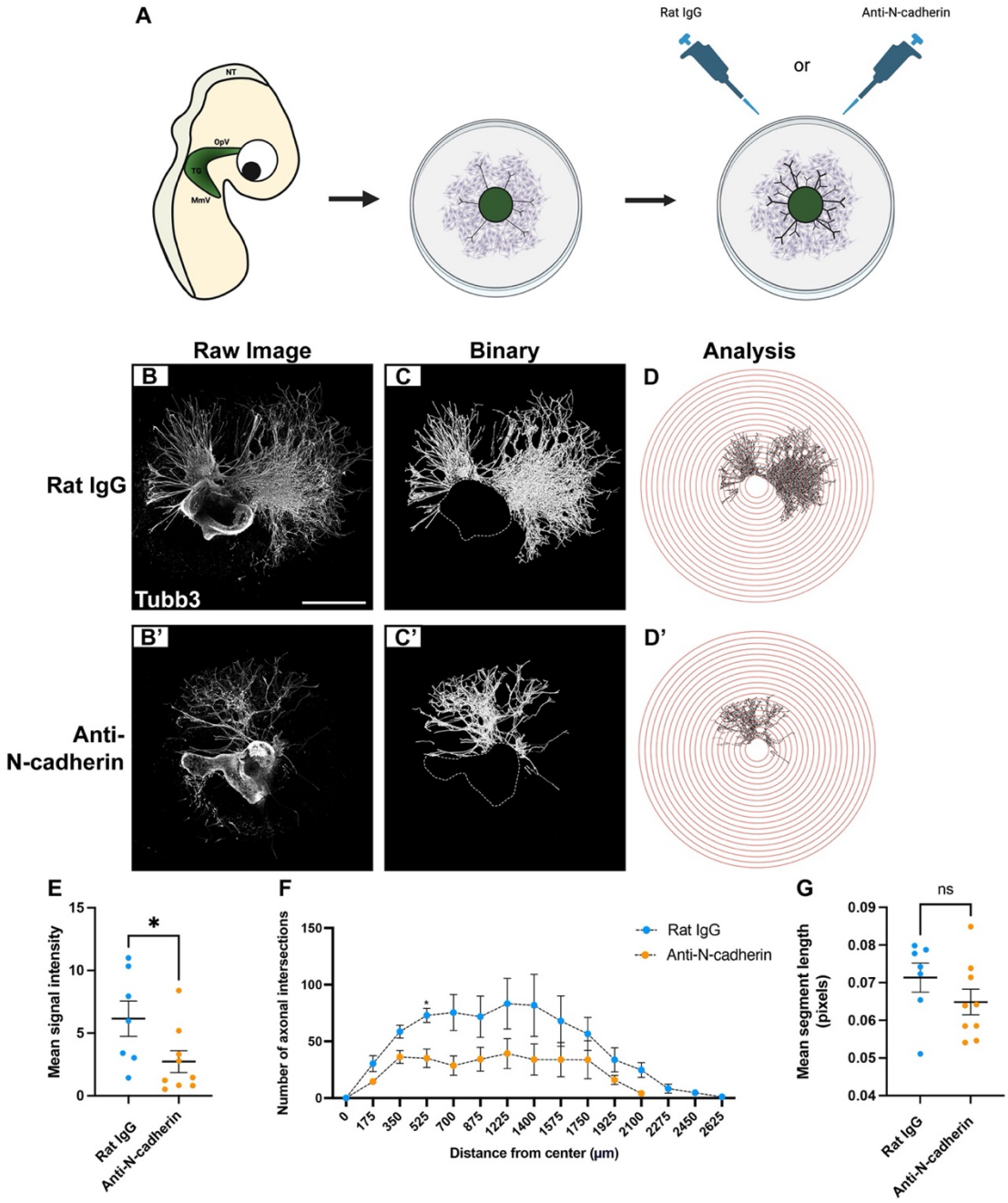
A
NT
OpV
TG
MmV
Rat IgG
or
Anti-N-cadherin
Raw Image
Binary
Analysis
B
C
D
Rat IgG
Tubb3
B'
C'
D'
Anti-
N-cadherin
E
Mean signal intensity
*
Rat IgG
Anti-N-cadherin
F
Number of axonal intersections
Rat IgG
Anti-N-cadherin
Distance from center (µm)
G
Mean segment length (pixels)
ns
Rat IgG
Anti-N-cadherin

Figure 3. Blocking the adhesive function of N-cadherin reduces trigeminal neuron axon outgrowth. (A) Schematic of N-cadherin function blocking assay. (B-C') Work-flow process for *in vitro* analyses. (B, B') Representative images of trigeminal ganglion explants after treatment with either control rat IgG (n=7) or anti-N-cadherin (n=9) antibody, respectively, followed by immunostaining for Tubb3. Scale bar in (B) is 1 mm and applies to (B'). (C, C') Generated binary images after ridge detection processing on Fiji for rat IgG- or anti-N-cadherin-treated explants, respectively. Dotted lines indicate perimeter of explanted tissue that was cropped during processing. (D, D') Processed images overlaid with concentric circle function to count the number of axonal intersections. (E) Mean signal intensity ± SEM of explant outgrowth following treatment with rat IgG or anti-N-cadherin. (E) Intersection analysis calculating the number of axonal intersections across concentric circles of increasing diameter, presented as mean ± SEM. (F) Mean segment length ± SEM, where segments are considered as individual axons in each explant image after rat IgG or anti-N-cadherin treatment. Statistical significance was determined via unpaired t-tests (E-G) with adjustments made for multiple comparisons (E). (*) $p<0.05$.

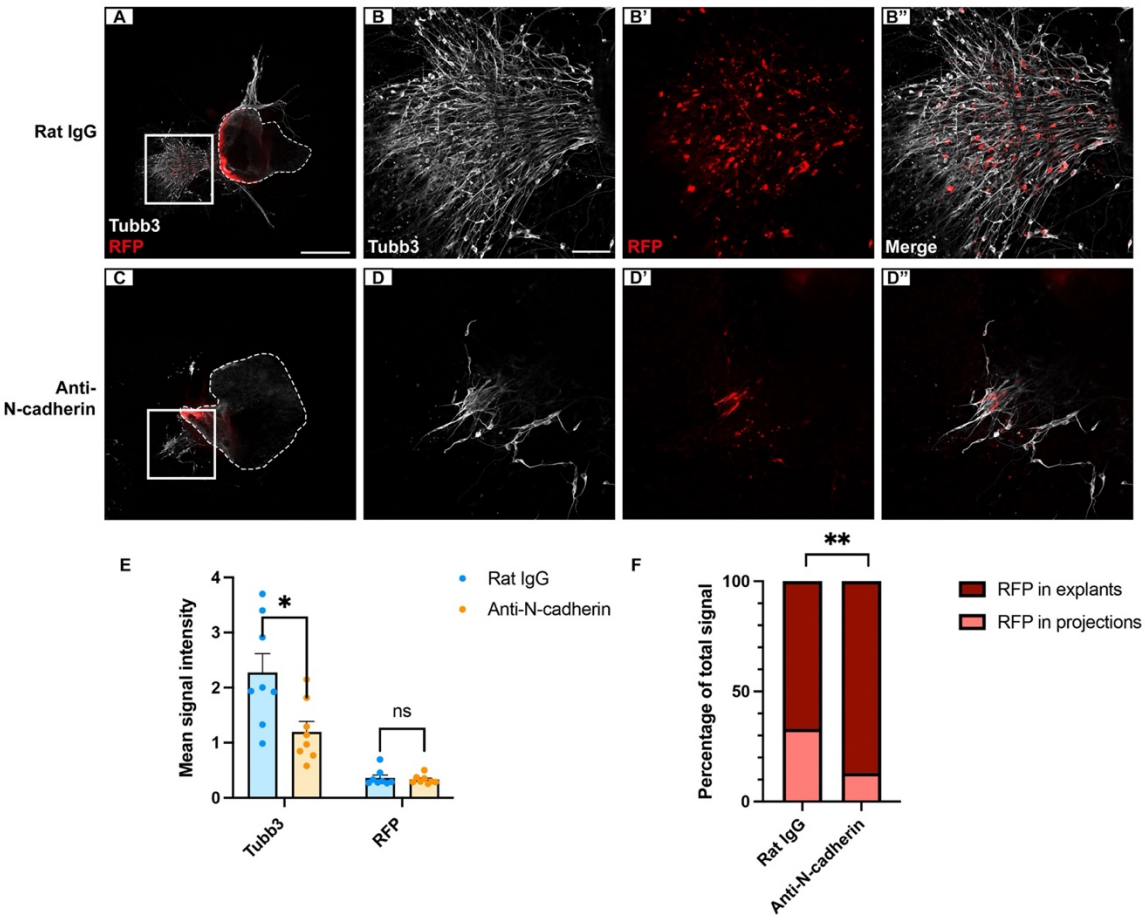

Figure 4. A subset of placodal neurons is able to extend axons independently of N-cadherin function. (A-D") Representative images of trigeminal explants with RFP-labeled placodal neurons after rat IgG (A-B", n=8) or anti-N-cadherin (C-D", n=8) treatment and immunostaining for RFP and Tubb3. Box in (A) and (C) indicates higher magnification images in (B-B"), and (D-D"), respectively. Dotted lines in (A) and (C) indicate perimeter of explanted tissue. Scale bar in (A) is 500 µm and applies to (C). Scale bar in (B) is 100 µm and applies to (B'-B", D-D"). (E) Mean signal intensity ± SEM for Tubb3 and RFP after rat IgG and anti-N-cadherin treatment. (F) RFP percent signal distribution between explants and axonal projections. Measurements for each condition (RFP in explants and RFP in projections after rat IgG and anti-N-cadherin treatment) were averaged and converted to percentages to yield percent distribution out of total RFP signal. Statistical significance was determined via the Mann-Whitney test (E) and Fisher's exact test (F). (*) $p<0.05$, (**) $p<0.01$.

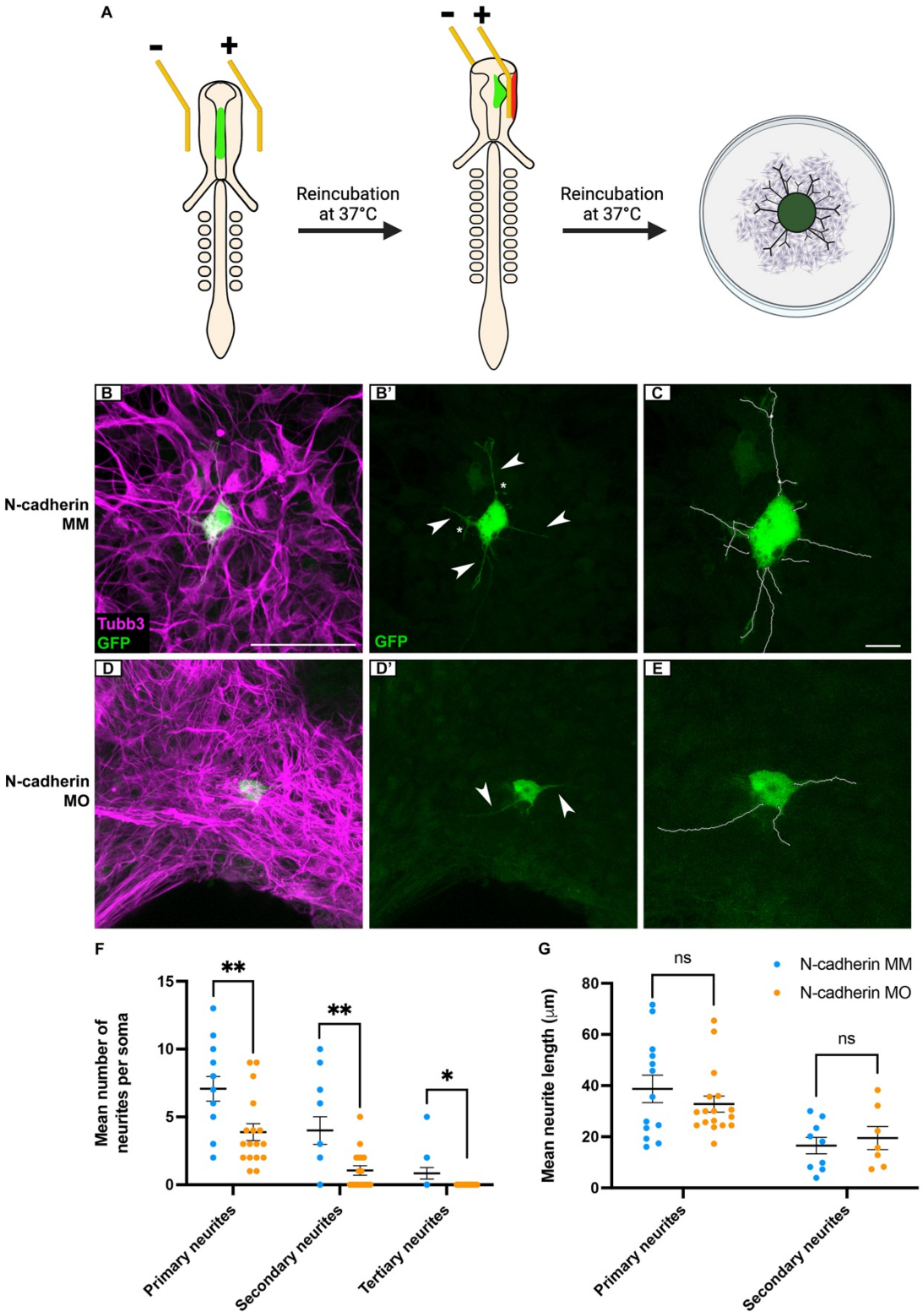
A
-
+
Reincubation at 37°C
Reincubation at 37°C
N-cadherin MM
N-cadherin MO
B
B'
C
D
D'
E
Tubb3
GFP
GFP
F
Mean number of neurites per soma
**
**
*
Primary neurites
Secondary neurites
Tertiary neurites
G
Mean neurite length (μm)
ns
ns
N-cadherin MM
N-cadherin MO
Primary neurites
Secondary neurites

Figure 5. N-cadherin depletion from placode cells decreases neurites and neurite complexity in neural-crest derived neurons. (A) Schematic of sequential electroporation explant culture technique. (B-E) Representative maximum intensity Z-projections of GFP-labeled neural crest-derived neurons after placodal electroporation with N-cadherin MM (B-B', n=13) or N-cadherin MO (D-D', n=17) taken from trigeminal ganglion explants following immunostaining for GFP and Tubb3, and neurite-traced images (C, E). Arrowheads and asterisks denote examples of primary and secondary neurites, respectively. Scale bar in (B) is 50 μm and applies to (B', D, D'). Scale bar in (C) is 10 μm and applies to (E). (F) Mean number ± SEM of GFP-positive neural crest-derived primary, secondary, and tertiary neurites after N-cadherin MM or N-cadherin MO electroporation. (G) Mean length ± SEM of GFP-positive neural crest-derived primary and secondary neurites after N-cadherin MM or N-cadherin MO electroporation. Statistical significance was determined via unpaired t-tests (D-E). (*) $p<0.05$, (**) $p<0.01$. ns: not significant.